Kinematics and stiffness of a planar tensegrity parallel mechanism

Zhifei Ji, *Tuanjie* Li, *Min* Lin

Abstract

In this work, the kinematics and stiffness of a planar tensegrity parallel mechanism are investigated. The analytical solutions to the forward and reverse kinematics were found using an energy method. The singular configurations and workspaces were detailed. Afterwards, the stiffness of the mechanism was analyzed. It is demonstrated that the stiffness is at a local maximum when the mechanism is in stable equilibrium and at a local minimum when the mechanism is in unstable equilibrium. The stiffness distributions are approximately symmetric about a certain line inside the actuator and Cartesian workspaces. Large values of the actuator length should be selected for high stiffness applications. The singular configurations, workspaces and stiffness variations inside the actuator and Cartesian workspaces lay a foundation for the use of the mechanism.

Keywords

tensegrity · static analysis · kinematics · stiffness · mechanisms

Zhifei Ji
School of Electro-Mechanical Engineering,
Xidian University, P. O. Box 188, Xi'an 710071, China
e-mail: zfji18@163.com

Tuanjie Li
Min Lin
School of Electro-Mechanical Engineering,
Xidian University, Xi'an 710071, China

1 Introduction

The term tensegrity was created by Fuller [1]. It seems that he was inspired by Snelson's sculpture [2]. Tensegrity structures are formed by a combination of compressive components and tensile components. A detailed history of tensegrity systems (i.e. structures or mechanisms) was given by Motro [3]. Tensegrity systems are completely researched for two mainly applications. The first application is used as structures. For this application, tensegrity structures have some attractive characteristics such as light-weight, easily modeled, efficiency [4] and easily tunable [5]. Due to these characteristics, tensegrity structures have been proposed to be used as bridges [6-7], antennas [8], domes [9], etc. In addition, there are two main issues for the analysis of tensegrity structures. One is the form-finding problem, which corresponds to the computation of the equilibrium shape of tensegrity structures for a given set of physical parameters. In the literature, the form-finding problem has been researched by many approaches [10-14]. Moreover, a review of form-finding methods was provided by Tibert and Pellegrino [15]. The other issue is the investigation of the structure behaviors under external loads [16]. Furthermore, a review of the static analysis of tensegrity structures was given by Juan and Tur [17].

The other application of tensegrity systems is used as mechanisms. Oppenheim and Williams [18] were the first to consider the actuation of tensegrity systems by modifying the lengths of their components in order to obtain tensegrity mechanisms. Afterwards, Knight et al. [19] showed that a triangular tensegrity prism had instantaneous mobility. This is a characteristic of all tensegrity prisms. Carane III et al. [20] performed the static analysis of an antiprism tensegrity mechanism using the virtual work approach. Mirats-Tur and Camps [21] studied the kinematics and statics of a three-bar tensegrity prism. Arsenault and Gosseline [22] proposed an "X" shape tensegrity mechanism and studied the kinematics and dynamics of the mechanism. In the past decade, some applications of tensegrity mechanisms have been proposed, such as tensegrity flight simulator [23], a tensegrity space telescope [24] and a tensegrity robot [25-27]. The investigation of tensegrity mechanisms can be divided into

two branches. First one is the study of tensegrity non-parallel mechanisms, and the second one is the study of tensegrity parallel mechanisms. Up to present, many works have focused on the analysis of tensegrity non-parallel mechanisms. However, just a few works have devoted on the study of tensegrity parallel mechanisms. A tensegrity parallel mechanism is composed of two platforms (a mobile platform and fixed platform) connected by a set of prismatic actuators and springs. The use of springs allows the mobile platform to generate translational and rotational movements with actuators locked. Due to this attractive nature, tensegrity parallel mechanisms can be possibly used as rides at amusement parks. Regarding tensegrity parallel mechanisms, the kinematics and dynamics [28-33] have been extensively researched. Little literature however has been found on the research of workspaces and stiffness of tensegrity parallel mechanisms. The main objective of this paper is to investigate the kinematics, workspaces and stiffness of a planar tensegrity parallel mechanism.

2 Mechanism Description

A diagram of the mechanism considered here is shown in Figure 1. It can be seen that the mobile platform consists of three struts D_1D_2, D_2D_3 and D_1D_3 while the base platform consists of three struts C_1C_2, C_1C_3 and C_2C_3. The prismatic actuator is used to vary the distance between nodes C_1 and D_1. The constituent components of the mechanism connected to each other at each node by 2-d rotational joints with frictionless and the whole mechanism lies in a horizontal plane. In Figure 1, nodes C_1, C_2 and C_3 are fixed to the ground and the Cartesian coordinate system $A(X, Y)$ is attached to node C_1.
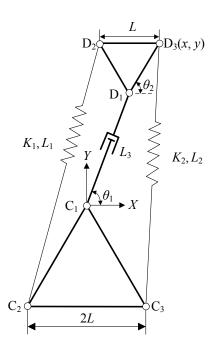

Fig. 1. A planar tensegrity parallel mechanism

As illustrated in Figure 1, the struts D_1D_2, D_1D_3 and D_2D_3 have the same length L while the struts C_1C_2, C_1C_3 and C_2C_3 have the same length $2L$. The angle between the X axis and the prismatic actuator C_1D_1 is defined as θ_1 while the angle between the X axis and the rigid strut D_1D_3 is defined as θ_2. The length of the prismatic actuator C_1D_1 is denoted by L_3. The springs are linear with stiffness K_i and lengths L_i (i = 1, 2). It is assumed that the springs have zero free lengths. This hypothesis is not problematic since, as was explained by Gosselin [34] and Shekarforoush et al. [35], virtual zero-free-length spring can be created by extending the actual spring beyond its attachment point.

The mobile platform has in general three linearly independent instantaneous freedoms measured relative to the base platform and is said to have three degrees of freedom. However, when the mechanism is in equilibrium, its potential energy is at its local minimum or maximum. Considering this constraint, we may say that the mechanism has two degrees of freedom when it is in equilibrium. Therefore, two descriptive parameters are needed to define the system. The variables of L_3 and θ_1, controlled by the actuators, are chosen as the inputs of the mechanism. The Cartesian coordinates of node D_3 are chosen as the outputs of the mechanism. The y coordinate of node D_1 is always chosen to be positive. For this reason, $0 \le \theta_1 \le \pi$. The range imposed to θ_2 is also chosen as $0 \le \theta_2 \le \pi$.

If the prismatic actuator is replaced by a line generator, the mechanism shown in Figure 1 can be used as a wave energy harvester. Suppose the mobile platform $D_1D_2D_3$ is connected with a float, the mobile platform $D_1D_2D_3$ can obtain kinematic energy from water waves. By using the line generator, the kinematic energy of the system can be changed into electric energy. This possible application is attractive since the water wave energy is clean and recycled.

3 Kinematic analysis

For a tensegrity mechanism, the kinematics and statics should be considered simultaneously since the shape of the mechanism depends not only on the mechanism's geometry but also on the internal forces in the springs. Therefore, it is assumed that the mechanism is always in equilibrium.

3.1 Forward Kinematic analysis

The forward kinematic analysis consists in computing the Cartesian coordinates of node D_3 for the given parameters (L_3 and θ_1).

From Figure 1, the coordinates of nodes C_1, C_2, C_3, D_1 and D_2 can be easily obtained as follows.

$$\mathbf{P}_{C_1} = \begin{bmatrix} 0 \\ 0 \end{bmatrix}, \ \mathbf{P}_{C_2} = \begin{bmatrix} -L \\ -\sqrt{3}L \end{bmatrix}, \ \mathbf{P}_{C_3} = \begin{bmatrix} L \\ -\sqrt{3}L \end{bmatrix},$$

$$\mathbf{P}_{D_1} = \begin{bmatrix} L_3 \cos\theta_1 \\ L_3 \sin\theta_1 \end{bmatrix}, \ \mathbf{P}_{D_2} = \begin{bmatrix} L_3 \cos\theta_1 + L\cos(\theta_2 + \frac{\pi}{3}) \\ L_3 \sin\theta_1 + L\sin(\theta_2 + \frac{\pi}{3}) \end{bmatrix} \quad (1)$$

Since the coordinates of node D_3 are chosen to be the output variables, thus we have

$$x = L_3 \cos\theta_1 + L\cos\theta_2 \quad (2)$$

$$y = L_3 \sin\theta_1 + L\sin\theta_2 \quad (3)$$

With the coordinates of all the nodes of the mechanism now known, the lengths of both springs can be easily expressed as a function of L_3, θ_1 and θ_2. As a consequence, the potential energy of the mechanism can be written as follows.

$$U = \frac{K_1 + K_2}{2}(5L^2 + L_3^2 + 2\sqrt{3}LL_3 \sin\theta_1)$$
$$+ (K_1 - K_2)LL_3 \cos\theta_1$$
$$+ [(2K_1 - K_2)L^2 + (\frac{K_1}{2} + K_2)LL_3 \cos\theta_1 + \frac{\sqrt{3}}{2}K_1LL_3 \sin\theta_1]\cos\theta_2$$
$$+ [(\frac{K_1}{2} + K_2)LL_3 \sin\theta_1 - \frac{\sqrt{3}}{2}K_1LL_3 \cos\theta_1 + \sqrt{3}K_2L^2]\sin\theta_2$$
$$(4)$$

When the mechanism is in equilibrium, its potential energy is at a local maximum or local minimum. Therefore, by differentiating U with respect to θ_2 and equating the result to zero, we have

$$\tan\theta_2 = \frac{\eta_1}{\eta_2} \quad (5)$$

where

$$\eta_1 = (K_1 + 2K_2)L_3 \sin\theta_1 - \sqrt{3}K_1L_3 \cos\theta_1 + 2K_2\sqrt{3}L \quad (6)$$

$$\eta_2 = 2(2K_1 - K_2)L + (K_1 + 2K_2)L_3 \cos\theta_1 + \sqrt{3}K_1L_3 \sin\theta_1 \quad (7)$$

Due to the range imposed to θ_2, computing the arctangent of Eq. (5) generates a unique solution. By substituting the solution for θ_2 into Eq. (2) and (3), a solution to the forward kinematic analysis is found.

3.2 Inverse kinematic analysis

The inverse kinematic analysis of the mechanism corresponds to the computation of the input variables (L_3 and θ_1) for the given coordinates of node D_3.

From Eqs. (2) and (3), the expression for $\tan\theta_2$ can be derived.

$$\tan\theta_2 = \frac{y - L_3 \sin\theta_1}{x - L_3 \cos\theta_1} \quad (8)$$

Eliminating the variable θ_2 from Eqs. (2) and (3), we obtain

$$E_1 L_3^2 + E_2 L_3 + E_3 = 0 \quad (9)$$

where

$$E_1 = 1, \ E_2 = -2(x\cos\theta_1 + y\sin\theta_1), \ E_3 = x^2 + y^2 - L^2 \quad (10)$$

Moreover, by combining the expression for $\tan\theta_2$ (see Eq. (8)) with Eq. (5), we have

$$F_1 L_3^2 + F_2 L_3 + F_3 = 0 \quad (11)$$

where

$$F_1 = \sqrt{3}K_1L$$
$$F_2 = L(K_1 + 2K_2)(x\sin\theta_1 - y\cos\theta_1)$$
$$\quad - \sqrt{3}L\cos\theta_1(K_1 x + 2K_2 L)$$
$$\quad + [2(2K_1 - K_2)L - \sqrt{3}K_1 y]L\sin\theta_1$$
$$F_3 = 2K_2 L^2 x - 2(2K_1 - K_2)L^2 y$$
$$(12)$$

Eqs. (9) and (11) can be considered as two quadratics with respect to L_3. Furthermore, according to Bezout's method [36], the condition that Eqs. (9) and (11) have a common root for L_3 is as follows.

$$\begin{vmatrix} E_1 & E_2 \\ F_1 & F_2 \end{vmatrix} \begin{vmatrix} E_2 & E_3 \\ F_2 & F_3 \end{vmatrix} - \begin{vmatrix} E_1 & E_3 \\ F_1 & F_3 \end{vmatrix}^2 = 0 \quad (13)$$

Moreover, the common root for L_3 can be computed using the following equation.

$$L_3 = -\frac{\begin{vmatrix} E_2 & E_3 \\ F_2 & F_3 \end{vmatrix}}{\begin{vmatrix} E_1 & E_3 \\ F_1 & F_3 \end{vmatrix}} \quad (14)$$

From Eq. (13), it can be seen that there is only one unknown θ_1 in Eq. (13). Therefore, the solution for θ_1 can be found by solving Eq. (13). By substituting Eqs. (10) and (12) into Eq. (13), we obtain

$$(\varphi_1 + \varphi_4)\tan^2\theta_1 + \varphi_2 \tan\theta_1 + \varphi_3 + \varphi_4 = 0 \quad (15)$$

where the coefficients φ_1 through φ_4 are detailed in Appendix A. The expression for $\tan\theta_1$ can be derived from Eq. (15) as follows.

$$\tan\theta_1 = \frac{-\varphi_2 \pm \sqrt{\varphi_2^2 - 4(\varphi_1 + \varphi_4)(\varphi_3 + \varphi_4)}}{2(\varphi_1 + \varphi_4)} \quad (16)$$

Since θ_1 is limited to the first two quadrants, computing the arctangent of Eq. (16) generates two solutions for θ_1. By substituting these results into Eq. (14), two solutions for L_3 can be arrived at. As a consequence, the solutions to the inverse kinematic analysis are found.

4 Singularity analysis
4.1 Mechanism Jacobian
For tensegrity mechanisms, the relationships between the input and output velocities can not be established since there are more degrees of freedom than actuators. However, due to the fact the mechanism is always assumed to be in equilibrium, its Jacobian, $\mathbf{J}$, can be defined as follows.

$$\mathbf{J} = \frac{\delta\mathbf{O}}{\delta\mathbf{I}} = \begin{bmatrix} \dfrac{\partial x}{\partial L_3} & \dfrac{\partial x}{\partial \theta_1} \\ \dfrac{\partial y}{\partial L_3} & \dfrac{\partial y}{\partial \theta_1} \end{bmatrix} \quad (17)$$

where $\mathbf{O} = [x, y]^\mathrm{T}$ and $\mathbf{I} = [L_3, \theta_1]^\mathrm{T}$. $\delta\mathbf{I}$ represents the infinitesimal changes of the mechanism's input variables while $\delta\mathbf{O}$ represents the infinitesimal changes of the mechanism's output variables. Using Eqs. (2) and (3), the elements of the Jacobian can be derived as follows.

$$\frac{\partial x}{\partial L_3} = \cos\theta_1 - L\sin\theta_2 \frac{\partial\theta_2}{\partial L_3} \quad (18)$$

$$\frac{\partial x}{\partial \theta_1} = -L_3\sin\theta_1 - L\sin\theta_2 \frac{\partial\theta_2}{\partial \theta_1} \quad (19)$$

$$\frac{\partial y}{\partial L_3} = \sin\theta_1 + L\cos\theta_2 \frac{\partial\theta_2}{\partial L_3} \quad (20)$$

$$\frac{\partial y}{\partial \theta_1} = L_3\cos\theta_1 + L\cos\theta_2 \frac{\partial\theta_2}{\partial \theta_1} \quad (21)$$

where

$$\frac{\partial\theta_2}{\partial L_3} = \cos^2\theta_2 \frac{\partial(\tan\theta_2)}{L_3}, \quad \frac{\partial\theta_2}{\partial\theta_1} = \cos^2\theta_2 \frac{\partial(\tan\theta_2)}{\theta_1} \quad (22)$$

We can compute the elements of $\mathbf{J}$ using Eqs. (18)-(21). As a consequence, the determinant of $\mathbf{J}$ can be obtained.

4.2 Singular configurations
The mechanism's singular configurations correspond to the situations where the determinant of $\mathbf{J}$ is zero, indeterminate and goes to infinity.

According to Eq. (17), the determinant of $\mathbf{J}$ can be derived as follows.

$$\det(\mathbf{J}) = \frac{L_3\Phi_1}{\Phi_2} \quad (23)$$

where

$$\begin{aligned}
\Phi_1 = &[(K_1 + 2K_2)L_3\sin\theta_1 \\
&-\sqrt{3}K_1L_3\cos\theta_1 + 2\sqrt{3}K_2L]\{[(K_1 + 2K_2)L_3\sin\theta_1 \\
&-\sqrt{3}K_1L_3\cos\theta_1 + 2\sqrt{3}K_2L]^2 + [2(2K_1 - K_2)L \\
&+(K_1 + 2K_2)L_3\cos\theta_1 + \sqrt{3}K_1 \\
&\cdot L_3\sin\theta_1]^2\} + 4L_3L\sin\theta_2(K_1 + 2K_2)[4L^2(K_1^2 + K_2^2 - K_1K_2) \\
&+L_3^2(K_1^2 + K_2^2 + K_1K_2) + 2L_3L\cos\theta_1(K_1^2 - K_2^2) \\
&+2\sqrt{3}L_3L\sin\theta_1(K_1^2 + K_2^2)]
\end{aligned} \quad (24)$$

$$\begin{aligned}
\Phi_2 = &[(K_1 + 2K_2)L_3\sin\theta_1 \\
&-\sqrt{3}K_1L_3\cos\theta_1 + 2\sqrt{3}K_2L]\{[(K_1 + 2K_2)L_3\sin\theta_1 \\
&-\sqrt{3}K_1L_3\cos\theta_1 + 2\sqrt{3}K_2L]^2 + [2(2K_1 - K_2)L \\
&+(K_1 + 2K_2)L_3\cos\theta_1 + \sqrt{3}K_1 \cdot L_3\sin\theta_1]^2\}
\end{aligned} \quad (25)$$

By analyzing the kinematic behaviors and examining Eqs. (23)-(25), the singular configurations and the corresponding expressions can be extracted.

i. $L_3 = 0$ (26)
- Node C_1 is coincident with node D_1.
- Finite movements of node D_3 in a direction perpendicular to the line joining nodes D_1 and D_3 are possible with actuators locked.
- Infinitesimal movements of node D_3 along a direction parallel to the line joining nodes C_1 and D_3 can not be generated.
- External forces applied in a direction perpendicular to the line joining nodes D_1 and D_3 can not be resisted by the actuators.
- The mechanism becomes uncontrolled. For this case, the equilibrium configurations of the mechanism do not depend on the value of θ_1.

ii. $\sin\theta_1 = 0$ (27)
- The node D_1 is located on the X axis.
- Finite movements of node D_3 perpendicular to the line joining nodes D_1 and D_3 are possible with actuators locked.
- Infinitesimal movements of node D_3 along a direction parallel to the line joining nodes D_1 and D_3 can not be generated.

- External torques applied to the mobile platform can not be resisted by the actuators.

iii. $(K_1 + 2K_2)L_3 \sin\theta_1 - \sqrt{3}K_1 L_3 \cos\theta_1 + 2\sqrt{3}K_2 L = 0$ (28)

- For this case, the determinant of **J** goes to infinity. Moreover, the mechanism becomes uncontrolled.

iv. $\theta_1 = \theta_2$ (29)

- Node D_3 is located on the line joining nodes C_1 and D_1.
- Finite movements of node D_3 perpendicular to the line joining nodes D_1 and D_3 are possible with actuators locked.
- Infinitesimal movements of node D_3 along a direction parallel to the line joining nodes D_1 and D_3 can not be generated.
- The external force applied to node D_3 along a direction parallel to the line joining nodes D_1 and D_3 can be resisted by the prismatic actuator $C_1 D_1$.

v. $\Phi_1 = 0$ (30)

- For this case, the determinant of **J** is zero. When this case occurs, infinitesimal movements of node D_3 perpendicular to the singular curve in the Cartesian workspace can not be generated. Generally, when the end-effector (node D_3) is fixed, the length L_3 and the angle θ_1 can also be changed by the actuators due to the use of springs. However, when $\Phi_1 = 0$, the input variables (L_3 and θ_1) can have infinitesimal changes without changing the lengths of the springs for a given position of node D_3. The case $\Phi_1 = 0$ corresponds a singular curve inside the actuator and Cartesian workspaces, as shown in Figs. 2 and 3.

5 Workspaces

The workspace of a mechanism is usually defined as the region that the end-effector can reach. However, it is interesting to investigate the ranges that the actuators can operate. We use the term actuator workspace to represent the ranges that the actuators can operate and the term Cartesian workspace to represent the region that the end-effector can reach. In this section, both workspaces have been studied respectively. The boundaries of a workspace and the singular curves in the workspace often correspond to the singular configurations of the mechanism. Based on this principle, the actuator workspace of the special tensegrity parallel mechanism can be mapped according to the singular configurations discussed in Section 4.2. Then, the Cartesian workspace can be obtained by mapping the boundaries and singular curves of the mechanism's actuator space into the Cartesian domain.

5.1 Actuator workspace

From Section 4.2, it can be observed that the expressions to which the singular configurations correspond can be considered as functions of variables L_3 and θ_1. In other words, the singular expressions detailed in Section 4.2 represent singularity curves or boundaries of the actuator workspace space. Therefore, by plotting these curves for a given set of mechanism parameters, the singularity curves as being part of the workspace boundary or being located inside the workspace can be determined. From Figure 1, it can be observed that the actuator workspace of the mechanism is an open set since the value of L_3 can go to infinity. However, this case (L_3 gose to infinity) is impossible when the planar tensegrity mechanism is put to use. For this reason, it is assumed that:

$$0 \leq L_3 \leq 2L \quad (31)$$

It is assumed that $L = 1$. The plot of the mechanism's actuator workspace is shown in Figure 2.
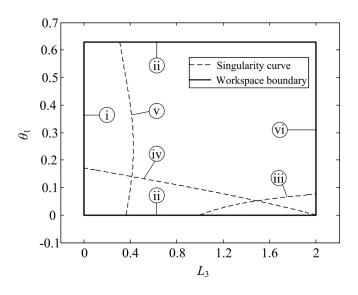

Fig. 2. Actuator workspace and singularity curves of the planar tensegrity mechanism with $K_1 = 200$ N/m, $K_2 = 100$ N/m.

Generally, in Figure 2, each curve can be identified according to the expressions of the singular configurations listed in Section 4.2. From Figure 2, it can be seen that curve vi does not correspond to any singular configuration. Curve vi corresponds to the limitation of the actuator length L_3 (see Eq. (31)). Furthermore, from Figure 2, it can also be observed that the singular configurations i and ii correspond to the boundaries of the actuator workspace while the singular configurations iii, iv and v correspond to the singular curves inside the actuator workspace.

In section 4.2, each singular configuration is expressed as a function of the variables L_3 and θ_1 except the singular configuration iv. Here, it is necessary to derive the expression for curve iv as a function of the variables L_3 and θ_1. By substituting the expression $\theta_1 = \theta_2$ into Eq. (5), we obtain

$$\tan\theta_1 = \frac{(K_1 + 2K_2)L_3 \sin\theta_1 - \sqrt{3}K_1 L_3 \cos\theta_1 + 2K_2\sqrt{3}L}{2(2K_1 - K_2)L + (K_1 + 2K_2)L_3 \cos\theta_1 + \sqrt{3}K_1 L_3 \sin\theta_1} \tag{32}$$

Simplifying Eq. (32) generates

$$2(2K_1 - K_2)L\sin\theta_1 - 2\sqrt{3}K_2 L\cos\theta_1 + \sqrt{3}K_1 L_3 = 0 \tag{33}$$

Eq. (33) is the expression to which curve iv in Figure 2 belongs. Since the singular curves and the boundaries of the actuator space correspond to the situations where the mechanism can not generate certain velocities of its end-effectors and actuators, the singular curves and the boundaries of the actuator space should be avoid when the mechanism is put to use. Also, the singular curves and the boundaries of the actuator space are of major importance during the design of such mechanism.

5.2 Cartesian workspace

By plotting the boundaries and singularity curves of the mechanism's actuator workspace into the Cartesian domain, the Cartesian workspace of the mechanism can be obtained. When the mechanism is in singular configurations, the expressions of the Cartesian workspace boundaries and singularity curves inside the Cartesian workspace can be extracted by analyzing the behaviors of the end-effector. Figure 3 shows the mechanism's Cartesian workspace complete with the identification of the different curves.
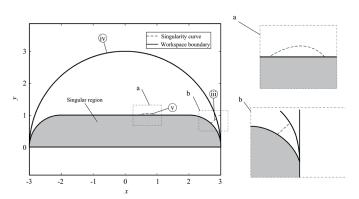

Fig. 3. Cartesian workspace and singularity curves of the planar tensegrity mechanism with $K_1 = 200$ N/m, $K_2 = 100$ N/m.

The expressions of the curves shown in Figure 3 are as follows.

i: $x^2 + y^2 = L^2$ (34)

ii: $\begin{cases} (x - L_3)^2 + y^2 = L^2 \\ 0 \leq L_3 \leq 2L \end{cases}$ (35)

iii: $2\sqrt{3}K_1 x - (K_1 + 2K_2)y + 2\sqrt{3}L(K_2 - K_1) = 0$ (36)

iv: $x^2 + y^2 = 9L^2$ (37)

From Section 4.2, we know that when the singular configuration ii occurs, the node D_1 is located on the X axis. The only possible movement of node D_3 is a rotation with respect to node D_1. Considering the range of L_3, it can be demonstrated that the singular configuration ii corresponds to a region which is shown in Figure 3. Importantly, it should be noted that the singular region contained the singularity curve i. The expressions for all the curves in Figure 3 can be obtained by analyzing the behaviors of the end-effector (node D_3). The exceptions to this rule are curves iii and v. For curve iii, by substituting the expression for the singular configuration iii (see Section 4.2) into Eq. (5), it is found that the value of θ_2 is equal to zero when the mechanism is in singular configuration iii. As a consequence, Eqs. (2) and (3) reduce to

$$x = L_3 \cos\theta_1 + L \tag{38}$$

$$y = L_3 \sin\theta_1 \tag{39}$$

By substituting Eqs. (38) and (39) into Eq. (28), the equation corresponding curve iii inside the Cartesian workspace is derived.

Substituting Eqs. (2) and (3) into Eq. (5) and rearranging yields

$$[(K_1 + 2K_2)y - \sqrt{3}K_1 x + 2\sqrt{3}K_2 L]\cos\theta_2$$
$$- [2(2K_1 - K_2)L + (K_1 + 2K_2)x + \sqrt{3}K_1 y]\sin\theta_2 + \sqrt{3}K_1 L = 0 \tag{40}$$

By solving Eq. (40) for θ_2 and substituting the result, along with Eqs. (2) and (3), into Eq. (30), an expression relating x and y for curve v is obtained. Due to its length, the expression for curve v is not listed here.

6 Stiffness

The stiffness of a mechanism is defined as the ability to resist the deformation caused by external loads. For the planar tensegrity parallel mechanism, in order to study its stiffness, the relationship between its deformation and the corresponding loads should be firstly developed.

6.1 Stiffness analysis with L_3 and θ_1 kept constant

From Figure 1, it can be seen that the only possible movement of the end-effector (node D_3) is a rotation with respect

to node D_1 with both actuators locked. Therefore, a relation is sought between an external torque (τ) applied to the mobile platform $D_1D_2D_3$ and the corresponding deformation quantified by θ_2. τ is obtained by differentiating U (see Eq. (4)) with respect to θ_2 as follows.

$$
\begin{aligned}
\tau &= \frac{\partial U}{\partial \theta_2} \\
&= -[(2K_1 - K_2)L^2 + (\frac{K_1}{2} + K_2)LL_3 \cos\theta_1 \\
&\quad + \frac{\sqrt{3}}{2}K_1LL_3 \sin\theta_1]\sin\theta_2 \\
&\quad +[(\frac{K_1}{2} + K_2)LL_3 \sin\theta_1 - \frac{\sqrt{3}}{2}K_1LL_3 \cos\theta_1 \\
&\quad + \sqrt{3}K_2L^2]\cos\theta_2
\end{aligned}
\tag{41}
$$

Moreover, the stiffness K of the mechanism can be obtained as follows.

$$
\begin{aligned}
K &= \frac{\partial^2 U}{\partial \theta_2^2} \\
&= -[(2K_1 - K_2)L^2 + (\frac{K_1}{2} + K_2)LL_3 \cos\theta_1 \\
&\quad + \frac{\sqrt{3}}{2}K_1LL_3 \sin\theta_1]\cos\theta_2 \\
&\quad -[(\frac{K_1}{2} + K_2)LL_3 \sin\theta_1 \\
&\quad - \frac{\sqrt{3}}{2}K_1LL_3 \cos\theta_1 + \sqrt{3}K_2L^2]\sin\theta_2
\end{aligned}
\tag{42}
$$

From Eqs. (4), (41) and (42), it can be observed that the potential energy, external torque and stiffness can be considered as functions with respect to θ_2. Plots of U, τ and K are shown are shown in Figs. 4-6 with $L = 1$ m, $L_3 = 6$ m, $K_1 = 100$ N/m, $K_2 = 10$ N/m and $\theta_2 = \pi/10$.

From Figs. 5-6, it can be seen that the case $\tau = 0$ corresponds to the equilibrium configuration. Also, the case $\tau = 0$ means that there is no external torque applied on the mechanism. The equilibrium configuration is identified by θ_{2_m} while the configuration that the stiffness of the mechanism is equal to zero is identified by θ_{2_0}. As a consequence, the range of θ_2 can be obtained as $\theta_2 \in [\theta_{2\_0}, \pi]$ with the given parameters.

From Figure 6, it can be observed that the stiffness is at a maximum when the mechanism is in equilibrium. By comparing Figure 5 with Figure 6, it is found that an increase in the external torque τ led to a decrease in the stiffness of the mechanism. This case is due to the fact that the configuration identified by θ_{2_m} corresponds to a stable equilibrium type of the mechanism. The equilibrium types of conservative systems can be seen in [37].
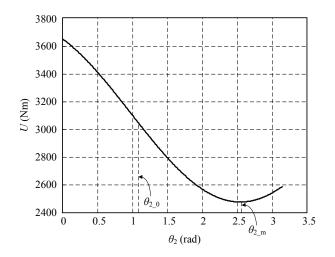

Fig. 4. The mechanism's potential energy as a function of θ_2 with $L_3 = 6$ m, $K_1 = 100$ N/m, $K_2 = 10$ N/m and $\theta_2 = \pi/10$.
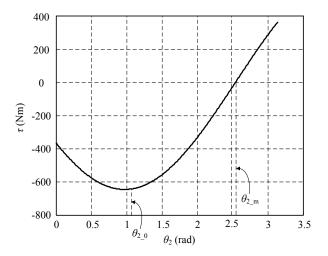

Fig. 5. The external torque as a function of θ_2 with $L_3 = 6$ m, $K_1 = 100$ N/m, $K_2 = 10$ N/m and $\theta_2 = \pi/10$.
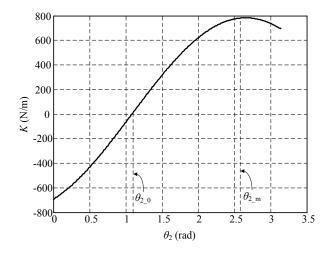

Fig. 6. The stiffness as a function of θ_2 with $L_3 = 6$ m, $K_1 = 100$ N/m, $K_2 = 10$ N/m and $\theta_2 = \pi/10$

From Eq. (4), the following expression can be obtain

$$\frac{\partial^{(j)}U}{\partial \theta_2^{(j)}} = -\frac{\partial^{(j+2)}U}{\partial \theta_2^{(j+2)}} \quad j = 1, 2, 3, \ldots \tag{43}$$

According to Eq. (43), we have

$$\frac{\partial K}{\partial \theta_2} = -\frac{\partial^3 U}{\partial \theta_2^3} = -\frac{\partial U}{\partial \theta_2} \tag{44}$$

$$\frac{\partial^2 K}{\partial \theta_2^2} = \frac{\partial^4 U}{\partial \theta_2^4} = -\frac{\partial^2 U}{\partial \theta_2^2} \tag{45}$$

The quantities in Eq. (44) are always equal to zero due to the fact that the potential energy is at its local minimum or local maximum when mechanism is in stable equilibrium or unstable equilibrium. Therefore, it can be demonstrated that the stiffness is always at a local minimum or local maximum. When the mechanism is in stable equilibrium, the potential energy is at a local minimum. The second derivative of U with respect to θ_2 is positive. For this case, it is found that the second derivative of K with respect to θ_2 is negative. Therefore, it can be concluded that K is always at a local maximum when the mechanism is in stable equilibrium. However, when the mechanism is in unstable equilibrium, the potential energy is at a local maximum. For this case, the second derivative of U with respect to θ_2 is negative. According to Eq. (45), we know that the second derivative of K with respect to θ_2 is positive. As a consequence, it can be obtained that the stiffness K is always at a local minimum when the mechanism is in unstable equilibrium. This rule is of major importance when such a mechanism is designed.

6.2 Stiffness distribution

In Section 6.1, the variation of the stiffness K along with the external torque was discussed when the actuators were locked (L_3 and θ_1 kept constant). It is demonstrated that the stiffness is at a local maximum when the mechanism is in stable equilibrium while it is at a local minimum when the mechanism is in unstable equilibrium. Moreover, when no torque is applied on the mechanism, the stiffness K varies along with the actuator parameters L_3 and θ_1. As a consequence, it is necessary to study the distribution of the stiffness K throughout the actuator and Cartesian workspaces with $\tau = 0$.

When the mechanism is in equilibrium, Eq. (5) should be satisfied. Considering the range imposed to θ_2, the following expression can be obtained from Eq. (5).

$$\sin \theta_2 = \sqrt{\frac{\eta_1^2}{\eta_1^2 + \eta_2^2}}, \quad \cos \theta_2 = \sqrt{\frac{\eta_1^2}{\eta_1^2 + \eta_2^2}} \cdot \frac{\eta_2}{\eta_1} \tag{46}$$

where the coefficients η_1 and η_2 are shown in Eqs. (6) and (7) respectively. Substituting Eq. (46) into Eq. (42) yields

$$K = -\sqrt{\frac{\eta_1^2}{\eta_1^2 + \eta_2^2}} \left\{ \left[(2K_1 - K_2)L^2 + (\frac{K_1}{2} + K_2)LL_3 \cos \theta_1 \right. \right.$$
$$\left. + \frac{\sqrt{3}}{2} K_1 LL_3 \sin \theta_1 \right] \cdot \frac{\eta_2}{\eta_1} + \left[(\frac{K_1}{2} + K_2)LL_3 \sin \theta_1 \right.$$
$$\left. \left. - \frac{\sqrt{3}}{2} K_1 LL_3 \cos \theta_1 + \sqrt{3}K_2 L^2 \right] \right\} \tag{47}$$

From Eq. (47), it can be observed that the stiffness K can be considered as a function of L_3 and θ_1. For a given set of mechanism's parameters, an example plot of the distribution of the stiffness K throughout the actuator workspace is shown in Figure 7.
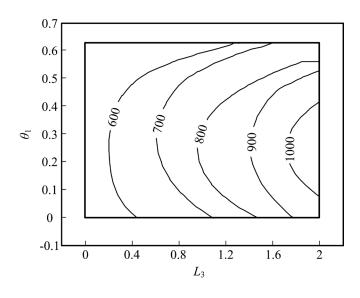
Fig. 7. Stiffness distribution in the actuator workspace for the planar tensegrity mechanism with $K_1 = 200$ N/m and $K_2 = 100$ N/m.

From Figure 7, it can be seen that the stiffness varies considerably throughout the actuator workspace. Furthermore, the stiffness increases with L_3. It can be demonstrated that large value of L_3 should be selected for high stiffness applications with the given mechanism's parameters. It can also be observed that the stiffness distribution curves are approximately symmetric with respect to the line $\theta_1 = 0.3$.

By mapping the stiffness distribution curves, shown in Figure 7, into the Cartesian domain, the stiffness distribution throughout the Cartesian workspace can be obtained. This can be done numerically. An example plot of the stiffness distribution in the Cartesian workspace is shown in Figure 8.

From Figure 8, it can be observed that the stiffness distribution is approximately symmetric with respect to the line $x = 0$. Moreover, when the x coordinate of the end-effector is specified, the stiffness increases with the y coordinate of the end-effector. For a given x, the stiffness increases with the y coordinate of node D_3. It can be concluded that large value of y should
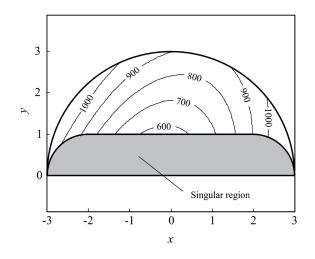
Fig. 8. Stiffness distribution in the Cartesian workspace for the planar tensegrity mechanism with $K_1 = 200$ N/m, $K_2 = 100$ N/m.

be considered when the mechanism is used for high stiffness applications.

Here, it is also important to derive the expression for K expressed by the variables x and y. Substituting Eqs. (2) and (3) into Eqs. (5) and (42), respectively, yields

$$\delta_1 \cos\theta_2 - \delta_2 \sin\theta_2 + \sqrt{3}K_1 L = 0 \qquad (48)$$

$$K = [(2K_1 - K_2)L^2 + (\frac{K_1}{2} + K_2)Lx - \frac{\sqrt{3}}{2}K_1 Ly]\cos\theta_2 +$$

$$[(\frac{K_1}{2} + K_2)Ly - \frac{\sqrt{3}}{2}K_1 Lx + \sqrt{3}K_2 L^2]\sin\theta_2 - (\frac{K_1}{2} + K_2)L^2$$

$$(49)$$

where

$$\delta_1 = (K_1 + 2K_2)y - \sqrt{3}K_1 x + 2\sqrt{3}K_2 L \qquad (50)$$

$$\delta_2 = 2(2K_1 - K_2)L + (K_1 + 2K_2)x + \sqrt{3}K_1 y \qquad (51)$$

Solving Eq. (48) for θ_2 and substituting the result into Eq. (49), we obtain

$$K = [(2K_1 - K_2)L^2 + (\frac{K_1}{2} + K_2)Lx - \frac{\sqrt{3}}{2}K_1 Ly]$$

$$\cdot\cos(2\tan^{-1}\frac{\delta_2 + \sqrt{\delta_1^2 + \delta_2^2 - 3K_1^2 L^2}}{\sqrt{3}K_1 L - \delta_1})$$

$$+[(\frac{K_1}{2} + K_2)Ly - \frac{\sqrt{3}}{2}K_1 Lx$$

$$+\sqrt{3}K_2 L^2]\sin(2\tan^{-1}\frac{\delta_2 + \sqrt{\delta_1^2 + \delta_2^2 - 3K_1^2 L^2}}{\sqrt{3}K_1 L - \delta_1})$$

$$-(\frac{K_1}{2} + K_2)L^2$$

$$(52)$$

Eq. (52) gives an analytical expression for the stiffness as a function of the variables x and y. Furthermore, for a given set of mechanism's parameters, the stiffness distribution in the Cartesian workspace can also be derived by plotting the stiffness (see Eq. (52)) throughout the Cartesian workspace.

7 Conclusion

In this work, the kinematics, workspaces and stiffness of a planar tensegrity parallel mechanism composed of two equilateral triangular platforms are studied. The analytical solutions to the forward and reverse kinematic analysis were found. Afterwards, the Jacobian of the mechanism was computed and the singular configurations were discussed. The actuator and Cartesian workspaces of the mechanism were mapped respectively. The singular curves inside the actuator and Cartesian workspaces were also detailed. The singular curves must be considered for mechanism designers when such mechanism is being designed. The stiffness of the mechanism was researched. It is demonstrated that when the mechanism is in stable equilibrium, the stiffness is at a local maximum and an increase in the external torque lead to a decrease in the stiffness. However, when the mechanism is in unstable equilibrium, the stiffness is at a local minimum. For this case, the stiffness increases with the external torque. In addition, the results of the analyses of stiffness distributions inside the actuator and Cartesian workspaces indicate that large L_3 may be selected for high stiffness applications. The stiffness distributions should be considered when the mechanism is put to use.

Appendix A. Details of coefficients φ_1 through φ_4.

Coefficients φ_1 through φ_4 appearing in Eq. (15) are as follows.

$$\varphi_1 = L[L(L^2 - x^2 - y^2)(4K_1L - 2K_2L + K_1x + 2K_2x - \sqrt{3}K_1y)$$
$$-4L^2 y(K_2y - 2K_1y + \sqrt{3}K_2x)]$$
$$(4K_1L - 2K_2L + K_1x + 2K_2x + \sqrt{3}K_1y)$$

$$\text{(C.1)}$$

$$\varphi_2 = [4L^3 y(K_2y - 2K_1y + \sqrt{3}K_2x)$$
$$+L^2(x^2 + y^2 - L^2)(4K_1L - 2K_2L + K_1x$$
$$+2K_2x - \sqrt{3}K_1y)]$$
$$(K_1y + 2K_2y + 2\sqrt{3}K_2L - \sqrt{3}K_1x)$$
$$-L[4L^2 x(K_2y - 2K_1y + \sqrt{3}K_2x)$$
$$-L(x^2 + y^2 - L^2)(K_1y + 2K_2y + 2\sqrt{3}K_2L + \sqrt{3}K_1x)]$$
$$\cdot(4K_1L - 2K_2L + K_1x + 2K_2x + \sqrt{3}K_1y)$$

$$\text{(C.2)}$$

$$\varphi_3 = L(x^2 + y^2 - L^2)(K_1y + 2K_2y + 2\sqrt{3}K_2L + \sqrt{3}K_1x)$$
$$-Ly(K_1 + 2K_2) - 4L^2 x(K_2y - 2K_1y + \sqrt{3}K_2x)$$
$$-2\sqrt{3}L^2K_2 + \sqrt{3}K_1Lx$$

$$\text{(C.3)}$$

$$\varphi_4 = -L^2[2\sqrt{3}K_2Lx - 2(2K_1 - K_2)Ly + \sqrt{3}K_1(L^2 - x^2 - y^2)]^2$$

$$\text{(C.4)}$$

References

1 **Fuller B.,** *Tensile-integrity structures*. United States Patent 3,063,521 (1962).

2 **Snelson K.,** *Continous tension, discontinuous compression structures*. United States Patent 316,961,116 (1965).

3 **Motro R.,** *Tensegrity systems: the state of the art*. International Journal of Space Structures, 7 (2), pp. 75-83, (1992).

4 **Bendsoe M., Kikuchi N.,** *Generating optimal topologies in structural design using a homogenization method*. Computer Methods in Applied Mechanics and Engineering, 71 (2), pp. 197-224, (1988). DOI: 10.1016/0045-7825(88)90086-2

5 **Chan W., Arbelaez D., Bossens F. et al.,** *Active vibration control of a three-stage tensegrity structures*. In: SPIE 11th Annual International Symposium on Smart Structures and Materials, San Diego 2004-3-15/18, (2004).

6 **Korkmaz S., Ali N. B. H., Smith I. F. C.,** *Configuration of control system for damage tolerance of a tensegrity bridge*. Advanced Engineering Informatics, 26 (1), pp. 145-155, (2012). DOI: 10.1016/j.aei.2011.10.002

7 **Rhode-Barbarigos L., Ali N. B. H., Motro R., Smith I. F. C.,** *Design Aspects of a Deployable Tensegrity-Hollow-rope Footbridge*. International Journal of Space Structures, 27 (2-3), pp. 81-96, (2012). DOI: 10.1260/0266-3511.27.2-3.81

8 **Fazli N., Albedian A.,** *Design of tensegrity structures for supporting deployable mesh antennas*, Scientia Iranica, 18 (5), pp. 1078-1087, (2011). DOI: 10.1016/j.scient.2011.08.006

9 **von Krüger P. G., Rodrigues F. C., Moreira L. E., Mantilla Carrasco E. V., Greco M.,** *Mechanical behavior of a tensegrity dome*. Mechnics Research Communications, 35 (7), pp. 460-465, (2008). DOI: 10.1016/j.mechrescom.2008.05.007

10 **Vassart N., Motro R.,** *Multiparametered form finding method: application to tensegrity systems*. International Journal of Space Structures, 14 (2), pp. 147-154, (1999).

11 **Koohestani K.,** *Form-finding of tensegrity structures via genetic algorithm*. International Journal of Solids and Structures, 49 (5), pp. 739-747, (2012). DOI: 10.1016/j.ijsolstr.2011.11.015

12 **Koohestani K., Guest S. D.,** *A new approach to the analytical and numerical form-finding of tensegrity structures*. International Journal of Solids and Structures, 50 (19), pp. 2995-3007, (2013). DOI: 10.1016/j.ijsolstr.2013.05.014

13 **Koohestani K.,** *A computational framework for the form-finding and design of tensegrity structures*. Mechanics Research Communications, 54, pp. 41–49, (2013). DOI: 10.1016/j.mechrescom.2013.09.010

14 **Zhang L.-Y., Li Y., Cao Y.-P., Feng X.-Q.,** *Stiffness matrix based form-finding method of tensegrity structures*. Engineering Structures, 58, pp. 36-48, (2014). DOI: 10.1016/j.engstruct.2013.10.014

15 **Tibert A. G., Pellegrino S.,** *Review of Form-Finding Methods for Tensegrity Structures*. International Journal of Space Structures, 26 (3), pp. 241-256, (2011). DOI: 10.1260/0266-3511.26.3.241

16 **Tran H. C., Lee J.,** *Geometric and material nonlinear analysis of tensegrity structures*. Acta Mechanica Sinica, 27 (6), pp. 938-949, (2011). DOI: 10.1007/s10409-011-0520-2

17 **Juan S. H., Tur J. M. M.,** *Tensegrity frameworks: Static analysis review.* Mechanism and Machine Theory, 43 (7), pp. 859-881, (2008). DOI: 10.1016/j.mechmachtheory.2007.06.010

18 Oppenheim I. J., Williams W. O., *Tensegrity prisms as adaptive structures*. In: Proceedings of the 1997 ASME International Mechanical Engineering Congress and Exposition, Dallas, USA, 1997-11-16/21, (1997).

19 Knight B., Zhang Y., Duffy J., Crane C., *On the line geometry of a class of tensegrity structures*. In: Sir Robert Stawell Ball 2000 Symposium, University of Cambridge, UK, July 2000, (2000).

20 Crane C. D., Duffy J., Correa J. C., *Static Analysis of Tensegrity Structures*. Journal of Mechanical Design, 127 (2), pp. 257-268, (2005). DOI: 10.1115/1.1804194

21 Mirats-Tur J. M., Camps J., *A Three-DOF Actuated Robot*. IEEE Robotics and Automation Magazine, 18 (3), pp. 96-103, (2011). DOI: 10.1109/MRA.2011.940991

22 Arsenault M., Gosselin C. M., *Kinematic, static and dynamic analysis of a planar 2-DOF tensegrity mechanism*. Mechanism and Machine Theory, 41 (9), pp. 1072-1089, (2006). DOI: 10.1016/j.mechmachtheory.2005.10.014

23 Sultan C., Corless M., Skelton R. E., *Tensegrity Flight Simulator*. Journal of Guidance, Control, and Dynamics, 23 (6), pp. 1055-1064, (2000). DOI: 10.2514/2.4647

24 Sultan C., Corless M., Skelton R. E., *Peak to peak control of an adaptive tensegrity space telescope*. In. Proceedings of SPIE-The International Society for Optical Engineering, Newport Beach, USA, 1999-3-1/4, (1999).

25 Paul C., Valero-Cuevas F. J., Lipson H., *Design and control of tensegrity robots for locomotion*. IEEE Transactions on Robotics, 22 (5), pp. 944-957, (2006). DOI: 10.1109/TRO.2006.878980

26 Offer S., Itay T., Bronfeld A. et al., *Adjustable tensegrity robot based on assur graph principle*. In: ASME 2009 International Mechanical Engineering Congress and Exposition, IMECE2009, Lake Buena Vista, USA, 2009-11-13/19, (2009).

27 Rovira A. G., Tur J. M. M., *Control and simulation of a tensegrity-based mobile robot*. Robotics and Autonomous Systems, 57 (5), pp. 526-535, (2009). DOI: 10.1016/j.robot.2008.10.010

28 Arsenault M., Gosselin C. M., *Kinematic, static and dynamic analysis of a spatial three-degree-of-freedom tensegrity mechanism*. Journal of Mechanical Design, 128 (5), pp. 1061-1069, (2005). DOI: 10.1115/1.2218881

29 Arsenault M., Gosselin C. M., *Kinematic and static analysis of 3-PUPS spatial tensegrity mechanism*. Mechanism and Machine Theory, 44 (1), pp. 162-179, (2009). DOI: 10.1016/j.mechmachtheory.2008.02.005

30 Bahman N. R. A., Mehrdad F., Mojtaba M., *Introducing and Analyzing a Novel Three-Degree-of-Freedom Spatial Tensegrity Mechanism*. Journal of Computational and Nonlinear Dynamics, 9 (2), 021017, (2014). DOI: 10.1115/1.4025894

31 Marshall M. Q., *Analysis of tensegrity-based parallel platform devices*. Master Thesis, University of Florida, Florida, USA, (2003).

32 Shekarforoush S. M. M., Eghtesad M., Farid M., *Kinematic and Static Analyses of Statically Balanced Spatial Tensegrity Mechanism with Active Compliant Components*. Journal of Intelligent & Robotic Systems, 71 (3-4), pp. 287-302, (2013). DOI: 10.1007/s10846-012-9784-4

33 Crane III C. D., Bayat J., Vikas V., Roberts R., *Kinematic Analysis of a Planar Tensegrity Mechanism with Pre-Stressed Springs*. In: Lenarčič, J., Wenger, P. (eds.), Advances in Robot Kinematics: Analysis and Design. Springer, Batz-sur-Mer, pp. 419-427, (2008). DOI: 10.1007/978-1-4020-8600-7_44

34 Gosselin C. M., *Static Balancing of Spherical 3-DOF Parallel Mechanisms and Manipulators*. International Journal of Robotics Research, 18 (8), pp. 819-829, (1999). DOI: 10.1177/02783649922066583

35 Shekarforoush S. M. M., Eghtesad M., Farid M., *Design of statically balanced six-degree-of-freedom parallel mechanisms based on tensegrity system*. In: 2009 ASME International Mechanical Engineering Congress and Exposition, Lake Buena Vista, USA, 2009-11-13/19, (2009).

36 Crane III C. D., Duffy J., *Kinematic Analysis of Robot Manipulators*. New York, Cambridge Press (1998).

37 Goldstein H., *Classical mechanics*. New Jersey, Addison-Wesley Press (1950).